

PACS numbers: 52.38.Kd; 52.38.Ph; 52.50.Jm; 42.65.Re
DOI: 10.1070/QE2009v039n07ABEH014024

Hot electron generation in a dense plasma by femtosecond laser pulses of subrelativistic intensity

V.V. Bol'shakov, A.A. Vorob'ev, D.S. Uryupina, K.A. Ivanov,
N. Morshedian, R.V. Volkov, A.B. Savel'ev

***Abstract*. We report a study of hot electron generation via the interaction of femtosecond laser pulses of subrelativistic intensity (10^{15} to 2×10^{17} W cm^{-2}), having different linear polarisations and nanosecond-scale contrasts, with the surface of 'transparent' (quartz glass) and 'absorbing' (silicon) targets. As the incident pulse intensity increases from 10^{15} to 10^{17} W cm^{-2}, the difference in hard X-ray yield and average hot electron energy between s- and p-polarised beams rapidly decreases. This effect can be understood in terms of relativistic electron acceleration mechanisms.**

Keywords: *femtosecond pulses, relativistic intensity, plasma, hot electrons.*

1. Introduction

The interaction of femtosecond laser pulses with the surface of a target produces a plasma in which the electrons have an essentially non-Maxwellian velocity distribution: in addition to thermal electrons, due to classical collisional mechanisms, there are hot electrons. It is the presence of hot electrons which underlies important effects such as the generation of hard X-ray radiation with a high spectral brightness and short pulse duration, acceleration of protons and multiply charged ions to high energies and nuclear reactions in the plasma.

The generation of hot electrons is due to additional (noncollisional) mechanisms of electron heating, and their average energy exceeds that of the thermal electrons by one to two orders of magnitude [1]. Hot electrons may account for 10 % to 30 % of the laser energy input [2, 3]. The mechanisms of hot electron generation at incident laser intensities below $(3 - 5) \times 10^{16}$ W cm^{-2} (so-called moderate intensity range) have been studied in sufficient detail both theoretically and experimentally [4, 5]. In this regime, the orientation of the linear polarisation of the incident radiation relative to the electron density gradient in the plasma is of considerable importance because, in the case of s-polarised radiation, the main mechanisms (anomalous skin effect [6, 7], resonance absorption [4, 8 – 10] and vacuum heating [8, 10, 11]) are inoperative, and no hot electrons are generated.

At incident intensities above the so-called relativistic intensity,* a key role in electron acceleration is played by the ponderomotive potential [1], $[\boldsymbol{v} \times \boldsymbol{B}]$ component of the Lorentz force [12, 13] and wake fields [14]. These mechanisms of hot electron generation have been intensely studied in the past decade, after the advent of techniques for producing relativistic intensities under laboratory conditions using relatively small laser systems. In particular, these mechanisms are insensitive to the orientation of the linear polarisation of the incident radiation but experience significant changes in going from linear to circular polarisation [15].

The intermediate range, covering subrelativistic intensities, where hot electron generation may be due to all the above mechanisms, has been studied in much less detail. In this intensity range, hot electrons can be produced by s-polarised radiation, and their energy distribution may have several peaks, due to different physical mechanisms.

Even at moderate incident intensities, the presence of a laser prepulse in the temporal radiation structure, with a prepulse intensity that may exceed the damage threshold of the target surface (10^{11} to 10^{13} W cm^{-2}, depending on the target material), has a significant effect on the interaction of femtosecond laser pulses with an overdense plasma. The main pulse then acts on a smoothed plasma – vacuum interface, whose width (the length scale of the electron density gradient) determines in significant part the main mechanism of hot electron generation. The influence of a laser prepulse is stronger at higher incident intensities, in particular, in all published reports on the interaction of relativistic laser pulses with matter, the prepulse intensity far exceeded the damage threshold of the target surface.

In this paper, we present a study of hot electron generation via the interaction of femtosecond laser radiation

V.V. Bol'shakov International Laser Center, M.V. Lomonosov Moscow State University, Vorob'evy gory, 119991 Moscow, Russia;
A.A. Vorob'ev International Laser Center, M.V. Lomonosov Moscow State University, Vorob'evy gory, 119991 Moscow, Russia;
A.M. Prokhorov General Physics Institute, Russian Academy of Sciences, ul. Vavilova 38, 119991 Moscow, Russia;
D.S. Uryupina, R.V. Volkov, A.B. Savel'ev International Laser Center, M.V. Lomonosov Moscow State University, Vorob'evy gory, 119991 Moscow, Russia; Department of Physics, M.V. Lomonosov Moscow State University, Vorob'evy gory, 119991 Moscow, Russia;
e-mail: ab_savelev@phys.msu.ru;
K.A. Ivanov, N. Morshedian Department of Physics, M.V. Lomonosov Moscow State University, Vorob'evy gory, 119991 Moscow, Russia

Received 17 December 2008; revision received 1 April 2009
Kvantovaya Elektronika **39** (7) 669 – 674 (2009)
Translated by O.M. Tsarev

*Intensity is referred to as relativistic when the oscillator velocity of electrons in an external electromagnetic field, $eE/(m\omega)$, approaches the speed of light.

of subrelativistic intensity (10^{15} to 2×10^{17} W cm^{-2}), having different linear polarisations and nanosecond-scale contrasts, with the surface of 'transparent' (quartz glass) and 'absorbing' (silicon) targets.

2. Experimental setup

In our experiments, we used the femtosecond Ti : sapphire laser system at the Multiuser Facility, International Laser Center, M.V. Lomonosov Moscow State University (MSU) [16] (pulse duration, 50 ± 5 fs, peak power, 0.2 TW, wavelength, 800 nm). In this laser system, the temporal contrast K on a nanosecond scale is determined by a laser prepulse which precedes the main pulse by 13 ns and has a factor of 4×10^6 smaller amplitude, and the picosecond-scale contrast is determined by a number of prepulses, the strongest of which precedes the main pulse by 7 ps and has a factor of 5×10^4 smaller amplitude. The relative level of the amplified spontaneous emission on a picosecond scale is within 10^5. The beam quality parameter M^2 is 1.8 ± 0.3.

The orientation of the linear polarisation of the incident radiation was varied using a half-wave plate. The nanosecond-scale contrast was controlled by turning off an extra Pockels cell, placed between the regenerative and multipass amplifiers, which reduced the contrast to 10^3. Further reduction in contrast, down to $K \sim 40$, was achieved by misaligning the polarisers of the Pockels cell of the regenerative amplifier. With this cell misaligned and the extra Pockels cell turned on, the contrast was 2×10^3.

The experimental arrangement is schematically illustrated in Fig. 1. The laser beam was focused onto the target by an aberration-free lens system (*2*) with a focal length of 6 cm, which ensured a spot diameter of ~ 4 μm. The peak intensity in our experiments was $\sim 2 \times 10^{17}$ W cm^{-2} at a pulse energy of 2 mJ. A flat solid target (*3*) was mounted at 45° to the laser beam axis. The target was secured to a two-axis positioning system in a vacuum chamber with a residual gas pressure of 10^{-2} Torr. During the experiment, the target was translated horizontally at a constant velocity so that it remained in the beam waist region. We examined laser pulse – target interaction at pulse repetition rates of 1 and 10 Hz.

To evaluate the average energy of hot electrons in the laser plasma, we measured the X-ray yield using energy filters in different spectral ranges with two photomultipliers (*5*) coupled to 5-mm-thick NaI(Tl) scintillator crystals. One X-ray detector, used to obtain a reference signal, measured the total X-ray yield over the entire energy range studied, 4-100 keV, for each laser shot. The other detector measured the X-ray yield in the energy range whose lower boundary was determined by the thickness of the aluminium filter placed in front of the detector and whose upper boundary was 100 keV. The dependence of the X-ray yield on the lower boundary of the filter passband at the 1/e level was fitted with an exponential, and the exponent was then used as an estimate of the average hot electron energy.

We used silicon (Si) and quartz glass (SiO_2) targets (*3*). The choice of these materials was prompted by the fact that, though close in average atomic weight, they differ in surface damage threshold by about one order of magnitude [17, 18] because glass is transparent, whereas silicon absorbs 800-nm radiation.

3. Experimental results and discussion

At an incident laser intensity of 2×10^{17} W cm^{-2}, we determined the average hot electron energy as a function of the orientation of the linear polarisation of the incident beam and also as a function of nanosecond-scale contrast at a pulse repetition rate of 10 Hz. Figure 2 shows the X-ray yield versus the lower energy of the filter passband at a nanosecond-scale contrast of 4×10^6. It can be seen that, in all instances, the experimental data is well fitted by an exponential. The data in Table 1 demonstrates that, under the conditions in question, hot electrons are effectively generated by s-polarised radiation as well and that the s- and p-polarisations differ only slightly in hard X-ray yield and average hot electron energy.

As mentioned above, at moderate incident intensities effective hot electron generation at planar interfaces is only possible in the case of p-polarised radiation, when there is a field component parallel to the electron density gradient. In this regime, hot electron generation by s-polarised radiation may result only from bending of the plasma – vacuum interface (or a surface at which the plasma electron concentration is of the order of the critical level). In

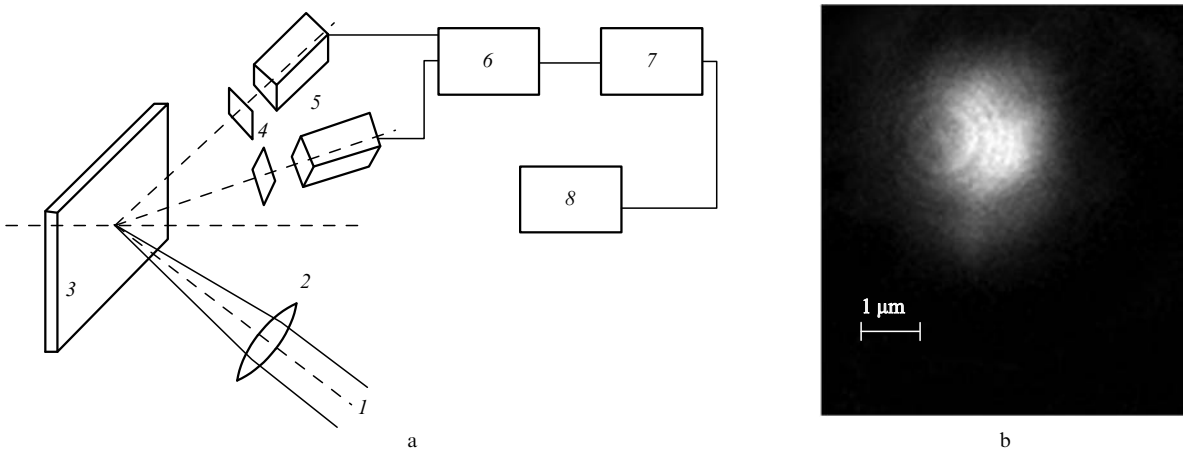

Figure 1. (a) Experimental arrangement and (b) image of the focal spot: (*1*) laser beam; (*2*) lens system; (*3*) target; (*4*) aluminium filters; (*5*) X-ray detectors; (*6*) charge-sensitive amplifier; (*7*) analog-to-digital converter; (*8*) computer.

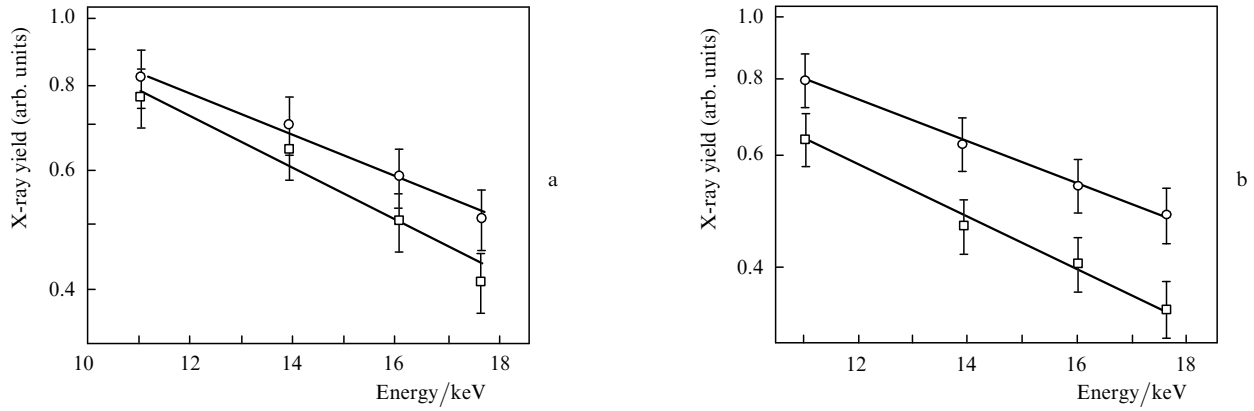

Figure 2. X-ray yield as a function of the lower energy of the filter passband and the estimated average hot electron energy for (a) Si and (b) SiO_2 targets at a nanosecond-scale contrast of 4×10^6 for (○) p- and (□) s-polarisations.

addition, the difference between the effects of p- and s-polarised radiation decreases or disappears in the relativistic regime.

In our experiments, a nonplanar interface may result from a spatial overlap of neighbouring exposed zones at a pulse repetition rate of 10 Hz. Figure 3 is a photograph of the silicon target surface after measurements at pulse repetition rates of 10 and 1 Hz. As seen, pulses with a repetition rate of 10 Hz produce a continuous track (groove), whereas at a repetition rate of 1 Hz each laser shot produces a separate crater. Therefore, at a repetition rate of 10 Hz each laser pulse impinges on a target surface partially modified by the preceding pulse, whereas at 1 Hz the target displacement is large enough for each pulse to encounter a virgin surface.

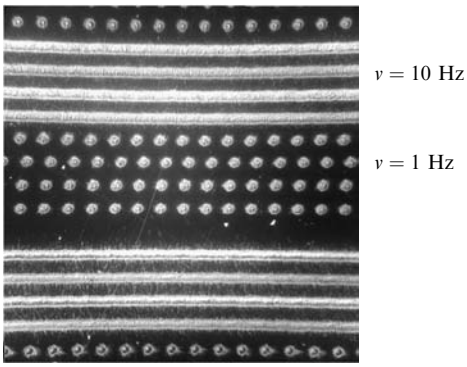

Figure 3. Photograph of the silicon target surface after measurements.

Table 1 lists the average hot electron energies for Si and SiO_2 targets at two pulse repetition rates and an incident intensity of 2×10^{17} W cm^{-2}. It follows from this data that, for both the s- and p-polarisations at pulse repetition rates of 1 and 10 Hz, the average hot electron energy depends little on the target material. Therefore, the slight variation in average hot electron energy is unrelated to bending of the plasma – vacuum interface.

Note that, in our experiments, the average hot electron energy increases systematically when the pulse repetition rate is reduced to 1 Hz, independent of the other beam parameters. The reduction in average hot electron energy

Table 1. Average energy of hot electrons produced by laser pulses with an intensity of 2×10^{17} W cm^{-2} incident on Si and SiO_2 targets at repetition rates of 1 and 10 Hz.

Target	Polarisation	ν/Hz	E/keV	
			$K = 4 \times 10^6$	$K = 10^2$
Si	p	1	18.2 ± 1.1	16.8 ± 1.0
	p	10	14.2 ± 0.9	11.5 ± 0.8
	s	1	16.0 ± 0.9	14.3 ± 0.9
	s	10	11.4 ± 0.8	10.6 ± 0.8
SiO_2	p	1	15.3 ± 0.9	18.1 ± 1.2
	p	10	13.1 ± 0.8	14.7 ± 0.9
	s	1	12.2 ± 0.8	15.7 ± 0.9
	s	10	10.4 ± 0.7	11.9 ± 0.8

upon multiple exposures of the same zone on the target surface is in contradiction with the reports [19, 20] that the hard X-ray yield and average hot electron energy increase when femtosecond laser pulses impinge on the same point on the target surface. In particular, this contradiction may be related to the continuous translation of the target in our experiments.

As mentioned above, an alternative explanation of the small difference in hard X-ray yield and average hot electron energy between the p- and s-polarised laser beams is that hot electron generation mechanisms essential at relativistic laser intensities come into play. In particular, at an incident laser intensity of $\sim 10^{17}$ W cm^{-2} the ponderomotive potential T_p reaches ~ 23 keV, which may lead to the generation of a considerable amount of hot electrons with an energy of the order of T_p, this effect being insensitive to the orientation of the linear polarisation of the incident laser beam.

To verify this assumption, we carried out a series of experiments in which plasma parameters were measured as a function of incident intensity at a nanosecond-scale contrast of 4×10^6 and pulse repetition rate of 10 Hz. The incident intensity was varied by displacing the focusing lens system from the perfect focusing position towards the target. The focal spot intensity was determined by standard formulas for a Gaussian beam [21], with the beam quality parameter taken into account.

Figure 4 plots the average hot electron energy, E, versus incident intensity, I, for silicon and quartz glass targets and two beam polarisations. In the range 10^{15} to 10^{16} W cm^{-2}, the average hot electron energy for p-polarised radiation

markedly exceeds that for s-polarised radiation, which correlates well with theoretical predictions and earlier experimental data [1]. In this intensity range, the average hot electron energy for p-polarised laser radiation incident on silicon and quartz glass increases with incident intensity as

$$E \approx (4.6 \pm 0.3)(I_{16}\lambda^2)^{0.35\pm0.02}, \quad (1a)$$

$$E \approx (4.1 \pm 0.1)(I_{16}\lambda^2)^{0.30\pm0.02}. \quad (1b)$$

respectively. Here, I_{16} is the intensity normalised to 10^{16} W cm^{-2}; λ is the laser wavelength in microns; and E is the energy in kiloelectronvolts. These formulas are in reasonable agreement with the known relation for the average energy of hot electrons produced by resonance absorption of laser radiation [1].

The slight differences between the coefficients and exponents in (1) may be due to the more effective hot electron generation in the case of silicon (which has a lower surface damage threshold) because of the more 'optimal' electron density gradient.

At $I \sim 10^{16}$ W cm^{-2}, the curves in Fig. 4 have a well-defined bend. The relations between the average hot electron energy and incident intensity take the form

$$E \approx (7.5 \pm 1)(I_{16}\lambda^2)^{0.13\pm0.03} \text{ (for Si)}, \quad (2a)$$

$$E \approx (5.0 \pm 0.4)(I_{16}\lambda^2)^{0.19\pm0.02} \text{ (for } SiO_2\text{)}. \quad (2b)$$

The break in the average hot electron energy as a function of incident intensity may be related to a change in the length scale of the ejection of the preplasma produced by the picosecond prepulse, because the prepulse intensity increases with main-pulse intensity. Moreover, at subrelativistic intensities resonance absorption may exhibit considerably more complex behaviour, and its efficiency may be substantially lower [22].

In the case of s-polarised incident radiation, hard X-ray radiation was detected at intensities above 4×10^{15} and 2×10^{16} W cm^{-2} for the silicon and fused quartz targets, respectively. These intensities are close to the surface damage thresholds of the target materials for picosecond prepulses with a temporal contrast of 2×10^3 [17, 18]. Figure 4 also illustrates the effect of incident intensity on the ratio of the average hot electron energies for p- and s-polarised beams. As seen, for $I > 10^{17}$ W cm^{-2} this ratio approaches unity for both targets. In this case, the relations between the average electron energy and incident intensity have the form

$$E \approx (2.3 \pm 0.1)(I_{16}\lambda^2)^{0.40\pm0.02} \text{ (for Si)}, \quad (3a)$$

$$E \approx (1.5 \pm 0.2)(I_{16}\lambda^2)^{0.38\pm0.04} \text{ (for } SiO_2\text{)}. \quad (3b)$$

Note that here the exponents for the two targets coincide and markedly exceed those in (1) and (2). As mentioned above, hot electron generation by an s-polarised laser beam may be due to effects that are essential at relativistic laser intensities. Since such mechanisms are as a rule effective at a smoothed plasma – vacuum interface, it seems likely that hot electrons are only generated at intensities above the surface damage threshold of the target for the prepulse.

In particular, as shown by Cai et al. [23], even at $I \sim 10^{17}$ W cm^{-2} hot electrons are ejected not along the polarisation of the incident laser beam but along the reflected beam. This finding indicates that 'relativistic' mechanisms play a significant role in hot electron acceleration even at this intensity.

The present results suggest that the preplasma produced by the prepulse plays an important role in the interaction between the plasma and femtosecond laser pulses with an intensity of $\sim 10^{17}$ W cm^{-2}. In the experiments considered above, a key role in preplasma generation was played by the picosecond prepulse, whose relative amplitude was determined by the characteristics of the laser system and did not vary. At the same time, our laser system allows the amplitude of the prepulse, preceding the main pulse by 13 ns, to be varied. In view of this, we measured the average hot electron energy as a function of nanosecond prepulse amplitude, or, what is the same thing here, as a function of nanosecond-scale contrast (Fig. 5).

A noteworthy feature of the data thus obtained is that, as the contrast of the p-polarised laser beam increases, the average hot electron energy rises systematically from 10 to 14 keV in the case of the Si target and decreases from 15 to 13.5 keV in the case of the SiO_2 target. In addition, the average hot electron energy for quartz glass at low pulse contrast coincides with that for silicon at high contrast, which indicates that the preplasma has similar character-

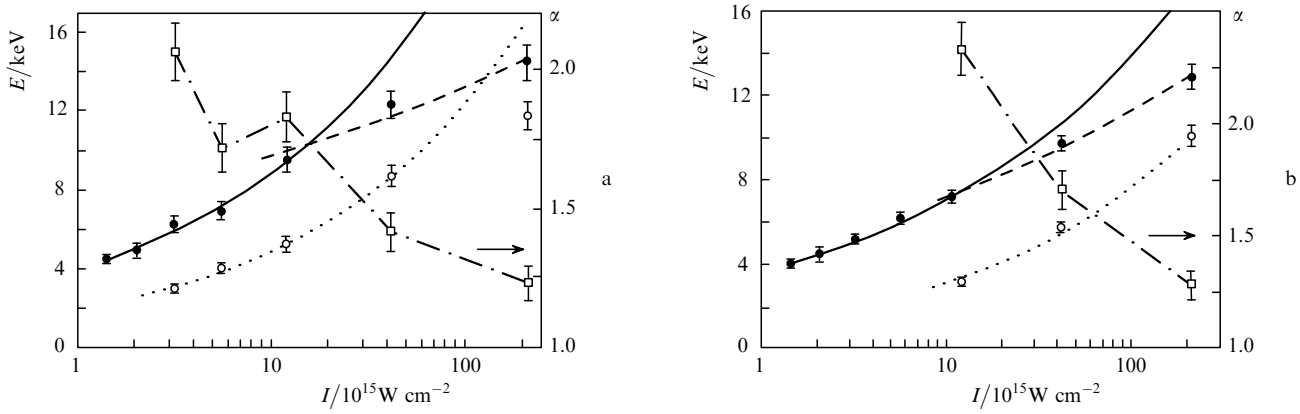

Figure 4. Effect of incident intensity, I, on the average hot electron energy, E, for p-polarised (● = experiment; solid and dashed lines = fits) and s-polarised (○ = experiment; dotted lines = fits) laser beams and on the ratio of the average hot electron energies for the p- and s-polarised beams, α (□ and dot-dashed lines): (a) Si target, (b) SiO_2 target; $K = 4 \times 10^6$.

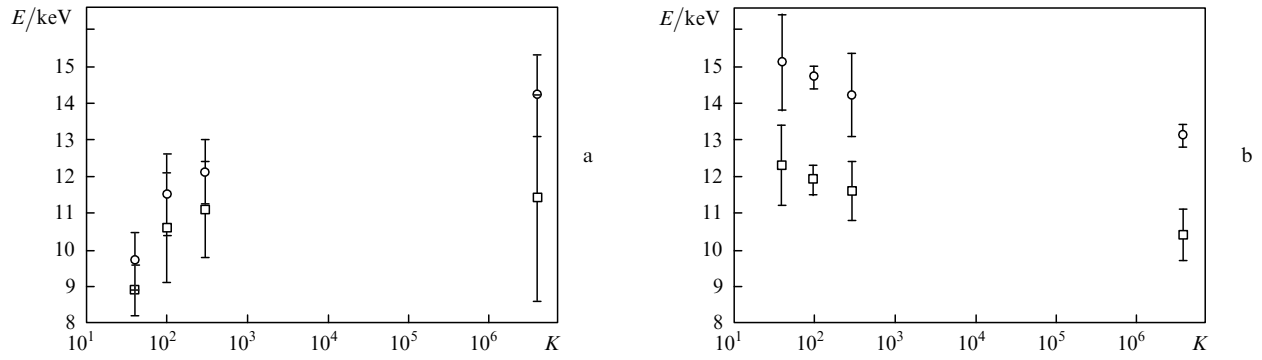

Figure 5. Average hot electron energy, E, as a function of nanosecond-scale contrast, K, for p- (○) and s-polarised (□) laser beams at $I = 2 \times 10^{17}$ W cm^{-2}: (a) Si target, (b) SiO_2 target.

istics under these conditions. It should be taken into account that, at $I = 2 \times 10^{17}$ W cm^{-2}, the picosecond prepulse intensity is also high.

In both instances, the average energy slightly decreases in going from the p- to s-polarisation, whereas the general trend remains unchanged. Thus, the slight difference between the s- and p-polarisations of the laser beam in this regime at the highest contrast (Fig. 4) persists at lower contrast.

In a separate experiment, the velocity of ions ejected from the plasma in various directions was measured for different beam polarisations using molten gallium as the target. As shown by Volkov et al. [24], the plasma produced by a laser pulse on the surface of liquids is identical in properties to that on the surface of solid targets. To measure ion currents, the vacuum chamber was connected to a time-of-flight mass spectrometer with a 28-cm flight tube, along the normal to the target surface or at 45° (along the reflected beam). Ion currents were measured with a VEU-7 chevron-configured microchannel-plate (MCP) detector. To ensure normal MCP operation and reduce the ion recombination probability on the path from the plasma to the detector, a vacuum of at least 10^{-5} Torr was maintained in the flight tube by a turbomolecular pump using a differential pumping system. Like in the experiments described above, the beam generated by the Ti : sapphire laser system was incident on the target surface at 45° to its normal. The experimental geometry was described in detail elsewhere [25].

As mentioned above, ion currents were measured for p- and s-polarisations in two directions. Data processing showed that slow ions had the highest velocity, $(5.7 \pm 0.3) \times 10^4$ m s^{-1}, along the normal to the target surface. This finding is consistent with the notion that particles are ejected from the plasma on the target surface in a large solid angle quasi-one-dimensionally along the normal to the surface. The velocity of fast ions ejected along the reflected beam was determined to be $(2.6 \pm 0.2) \times 10^6$ m s^{-1}, that is, almost twice the velocity of the ions ejected along the normal to the target surface: $(1.5 \pm 0.1) \times 10^6$ m s^{-1}. In addition, the velocity of both the fast and slow ions was found to be independent of the beam polarisation. This behaviour of ion currents suggests that the electron acceleration mechanisms essential at relativistic laser intensities come into play even at a pulse intensity of $\sim 10^{17}$ W cm^{-2}. Indeed, in the case of the hot electron acceleration mechanisms operative at moderate incident laser intensities (resonance absorption, vacuum heating and absorption in the anomalous skin effect regime), hot electrons are generated only by p-polarised laser pulses and are ejected along the normal to the target surface.

4. Conclusions

The present results on hot electron generation at incident intensities of up to 2×10^{17} W cm^{-2} with the use of transparent (quartz glass) and absorbing (silicon) targets demonstrate that, even at intensities about one order of magnitude below relativistic intensities, relativistic effects play a significant role in hot electron production. In particular, this leads to efficient hot electron generation even by s-polarised laser beams, with an average electron energy very close to that in the case of p-polarised radiation.

In the regime in question, the laser prepulse plays an important role, leading to a surface breakdown for both silica (transparent) and silicon targets and producing an extended electron density gradient. The gradient ensures predominance of resonance absorption in hot electron generation and effective operation of electron acceleration mechanisms that are essential at relativistic laser intensities: ponderomotive acceleration and heating by the $[v \times B]$ component of the Lorentz force. When the intensity of a prepulse that precedes the main pulse by several nanoseconds approaches the damage threshold, it also begins to play an important role, increasing the average hot electron energy in the case of transparent (silica) targets and reducing it in the case of absorbing (silicon) targets.

In conclusion, note that the present results of course provide no complete picture of hot electron generation at subrelativistic laser intensities. More in-depth experimental and theoretical studies, including numerical simulation, are needed to gain detailed insight into this process.

This work is the continuation of the studies initiated by S.A. Akhmanov at MSU as early as the late 1980s, which addressed the interaction of superstrong optical fields with matter and the associated generation of hot dense plasmas. One of us (A.B.S.) was fortunate to participate in those studies, under the capable direction of Sergei Aleksandrovich, a bright talent who could perfectly foresee global trends in scientific progress.

Acknowledgements. This work was supported by the Russian Foundation for Basic Research (Grant No. 07-02-00724a).

References

1. Gibbon P., Forster R. *Plasma Phys. Control. Fus.*, **38**, 769 (1996).
2. Soom B., Chen H., Fisher Y., Meyerhofer D.D. *J. Appl. Phys.*, **74**, 5372 (1993).
3. Rousse A., Audebert P., Geindre J.P., Fallies F., Gauthier J.C. *Phys. Rev. E*, **50**, 2200 (1994).
4. Brunel F. *Phys. Rev. Lett.*, **59**, 52 (1987).
5. Meyerhofer D.D., Chen H., Delettrez J.A., Soom B., Uchida S., Yaakobi B. *Phys. Fluids B*, **5**, 2584 (1993).
6. Andreev A.A., Gamaly E.G., Novikov V.N., Semakhin A.N., Tikhonchuk V.T. *Proc. SPIE Int. Opt. Soc. Eng.*, **1800**, 86 (1992).
7. Andreev A.A., Gamalii E.G., Novikov V.N., Semakin A.N., Tikhonchuk V.T. *Zh. Eksp. Teor. Fiz.*, **101**, 1808 (1992).
8. Forslund D.W., Kindel J.M., Lee K. *Phys. Rev. A*, **11**, 679 (1975).
9. Forslund D.W., Kindel J.M., Lee K. *Phys. Rev. Lett.*, **39**, 284 (1977).
10. Gibbon P., Bell A.R. *Phys. Rev. Lett.*, **68**, 1535 (1992).
11. Chen L.M., Zhang J., Dong Q.L., Teng H., Liang T.J., Zhao L.Z., Wei Z.Y. *Phys. Plasmas*, **8**, 2925 (2001).
12. Landau L.D., Lifshitz E.M. *The Classical Theory of Fields* (Oxford: Pergamon, 1975; Moscow: Fizmatlit, 2003).
13. Kruer W.L., Estabrook K. *Phys. Fluids*, **28**, 430 (1985).
14. Lehmann G., Laedke E.W., Spatschek K.H. *Phys. Plasmas*, **14**, 103109 (2007).
15. Li Y.T., Zhang J., Sheng Z.M., Zheng J., Chen Z.L., Kodama R., Matsuoka T., Tampo M., Tanaka K.A., Tsutsumi T., Yabuuchi T. *Phys. Rev. E*, **69**, 036405 (2004).
16. Bol'shakov V.V., Vorob'ev A.A., Volkov R.V., Knyaz'kov V.A., Eremin N.V., Paskhalov A.A., Shevel'ko A.P., Kazakov E.D., Romanovskii M.Yu., Savel'ev A.B. *Prikl. Fiz.*, **1**, 18 (2009).
17. Von der Linde D., Sokolowski-Tinten K., Bialkowski J. *J. Appl. Surf. Sci.*, **109**, 1 (1997).
18. Stuart B.C., Feit M.D., Herman S., Rubenchik A.M., Shore B.W., Perry M.D. *Phys. Rev. B*, **53**, 1749 (1996).
19. Golishnikov D.M., Gordienko V.M., Mikheev P.M., Savel'ev A.B., Volkov R.V. *Laser Phys.*, **11**, 1205 (2001).
20. Gordienko V.M., Makarov I.A., Rakov E.V., Savel'ev A.B. *Kvantovaya Elektron.*, **35** (6), 487 (2005) [*Quantum Electron.*, **35** (6), 487 (2005)].
21. Akhmanov S.A., Nikitin S.Yu. *Fizicheskaya optika* (Physical Optics) (Moscow: Nauka 2004; Oxford: Clarendon, 1997).
22. Xu Hui, Sheng Zheng-Ming, Zhang Jie, Yu M.Y. *Phys. Plasmas*, **13**, 123301 (2006).
23. Cai D.F., Gu Y.Q., Zheng Z.J., Zhou W.M., Yang X.D., Jiao C.Y., Chen H., Wen T.S., Chunyu S.T. *Phys. Rev. E*, **70**, 066410 (2004).
24. Volkov R.V., Gordienko V.M., Mikheev P.M., Savel'ev A.B., Uryupina D.S. *Kvantovaya Elektron.*, **34** (2), 135 (2004) [*Quantum Electron.*, **34** (2), 135 (2004)].
25. Uryupina D.S., Kurilova M.V., Morshedian N., Volkov R.V., Savel'ev A.B. *Vestn. Mosk. Univ., Ser. 3: Fiz. Astron.*, **4**, 39 (2008).